Synthesis and Characterization of InN Nanocrystals on Glass substrate by Plasma Assisted Reactive Evaporation

V. Ganesh[1 a)], M. Alizadeh[2], A. Shuhaimi[2] , S.Sundaram[3], K. M. Hakim[2], B. T. Goh[2] and S.A. Rahman[2]

[1] *Department of Physics and nanotechnology, SRM University, Kattankulathur, Chennai, India 603203*
[2] *Low Dimensional Materials Research Centre, Department of Physics, Faculty of Science, University of Malaya, 50603 Kuala Lumpur, Malaysia*
[3] *Georgia Tech Lorraine and CNRS, UMI2958, 57070 Metz, France*

[a)] Corresponding author:
Dr. V. Ganesh, DST-SERB Young scientist,
Department of Physics and Nanotechnology,
SRM University, Kattankulathur, Chennai, India
e-mail: ganeshuma2011@gmail.com, 80.vganesh@gmail.com
Phone: +918106562219

Abstract. InN nanocrystals were grown on glass substrate by plasma assisted reactive evaporation technique and the quality was compared with InN on Si (111) substrate. Single phase InN was confirmed by X-ray diffraction and micro Raman analysis on both the substrates. Agglomerated and Hexagonal faceting nanocrystals observed by field emission scanning electron microscopy. Energy dispersive X-ray analysis shows InN nanocrystals are nearly stochiometric. Photoluminescence reveals a broad emission near bandedge at 2 .04 eV and defect band at1.07 eV. The Hall measurement on both the substrates reveals high electron carrier concentration. These encouraging results obtained suggested that high quality single crystalline InN can be obtained on glass substrate further optimizing the growth parameters. This novel growth of InN nanocrystals on glass substrate is an important step towards the development of monolithic, high efficiency low-cost InGaN-based renewable energy sources.

Keywords: Plasma assisted reactive evaporation, XRD, FESEM, Micro Raman and PL

Introduction

Epitaxial growth of InN films attracts significant interest amongst other related nitride semiconductors due to it's tunable direct bandgap, high electron mobility, low effective mass for free electrons, high saturation velocity and high absorption coefficient which are interesting for applications like solar cells and other renewable energy sources [1]. Metal organic chemical vapor deposition (MOCVD) technique is commercially viable technique for the growth of GaN and its alloy based materials, this technique overcome certain challenges to grow InN like (high thermal decomposition) using lower growth temperature and high V/III ratio to avoid In droplets during the InN growth. Other promising methods are used to deposit single crystalline InN films are plasma assisted molecular beam of epitaxy [2], Molecular beam epitaxy (MBE) [3, 4]. Various other methods such as hydride vapor phase epitaxy (HVPE) [5], chemical vapor deposition [6], reactive d.c. magnetron sputtering [7] have been used to deposit mostly polycrystalline III-nitride films. These deposition methods listed above is not cost effective, researchers used ammonia for nitrogen source and also employed high decomposition temperature around 500 to 600 ºC [5]. In other words, preparation of thin films at low substrate temperatures simplifies deposition system, shortens time of the process and as a result makes it possible to gain higher throughput at low cost. Plasma assisted reactive evaporation can be employed in this work for deposition of InN films. The plasma assisted reactive evaporation system was built by combination of both hot wire chemical vapor deposition (HWCVD) and plasma enhanced chemical vapor

deposition (PECVD) systems. One of the most outstanding advantages of HWCVD is the high deposition rate [8] which is favorable for low-cost and large-scale industrial production. The hot filament (tungsten wire), as a versatile tool, can simultaneously evaporate In metal and effectively dissociates N_2 molecules into nitrogen atoms respectively. The evaporated In and N species gaining enough kinetic energy and travel towards substrate surface. The energized neutral species then can reach the substrate and release their thermal energy onto the top-most substrate surface upon hitting the surface, which in turn provides an internal heating channel [9,10]. Plasma is a well-known medium for generation of growth species and activation of surface bonds as well as effective post-processing of nanomaterials of a large variety of elements [11-13]. Also, a plasma discharge can effectively control the generation, transport and deposition of growth building units (BU) on an exposed-substrate surface [11-14]. Therefore, plasma assisted reactive evaporation, as a technique which encompasses all notions of hot-filament-led building unit generation and plasma-enabled BU generation and substrate heating could be a promising approach for deposition of InN thin films. Previously an InN film has been deposited using this method on Si (111) substrate [15].

InN material and its alloy system with direct bandgap are very promising for future renewable energy sources like water splitting cum hydrogen and solar cells, if we can lower the cost involved by avoiding sophisticated deposition tools, expensive precursors, and single crystalline substrates. This simple process demonstrated in this article eliminates all the above factors and has capabilities for industrial scaling-up with low cost of ownership. In general the III-nitride semiconductors are deposited on single crystalline substrates (sapphire, Si, SiC, etc..) which have shown good epitaxial match with them, however these substrates are expensive and have small wafer size, limiting their usage in large scale production. Considering the future applications of III- nitrides such as flat panel displays, photovoltaic's and hydrogen generation, large size and cheap substrates are key factors to reduce the system cost. So InN growth on low cost glass substrate is highly desired, because of its unlimited size and low manufacturing cost. In this study, we report the growth of high quality, single-phase InN nanocrystals using plasma assisted reactive evaporation method targeting the water splitting, hydrogen storage, and other novel renewable energy applications, in addition the characteristics of the material was studied and compared with that of InN films deposited on single crystalline Si (111) substrate.

2 Materials and Method

InN thin films are deposited on glass and Si (111) substrates simultaneously using custom-made plasma assisted reactive evaporation technique. The reactor consists of two parallel electrodes within a stainless steel chamber, the upper electrode served as gas showerhead, is connected to RF power of 13.56 MHz. The substrate holder was used as lower electrode and is grounded. The distance between the upper and grounded electrodes was 4.5 cm. A tungsten wire was used as filament and fixed at 1 cm above the substrate holder. Si and glass Substrate were cleaned with acetone and iso-propanol in ultrasonic bath for 10 min followed by rinsing with deionized water. The Si substrate is further cleaned with acids before loading in to the chamber (HCL solution, NH_4OH solution and HF aqua solution) to remove the native oxide from Si surface. Indium wire (diameter of 1 mm and length of 1 mm) with 99.999% purity was placed inside the tungsten filament. The reactor chamber was pumped down to a background pressure of 2×10^{-6} mbar. Substrate temperature was maintained at 250 $^{\circ}$C during the deposition using a rod type heater placed under the substrate holder. Hydrogen (H_2) plasma treatment was performed on the substrate at a constant flow rate of 100 sccm with RF power of 10W for 10 min prior to the deposition. Nitrogen (N_2) plasma was initiated by N_2 flow rate of 80 sccm and RF power of 100W. After N_2 plasma is stabilized, indium was evaporated by heating tungsten filament at a temperature of 1050 °C and the deposition time was 10 min. The pressure was maintained at 3.5×10^{-1} mbar during deposition.

The crystalline nature and structural properties of samples were studied using X-ray diffraction (XRD) by SIEMENS D5000 X-ray diffractometer (Cu Kα X-ray radiation λ = 1.5418 Å) and Micro-Raman Spectrometer (Renishaw Raman microscope) equipped with a laser source of Ar^+ with selected excitation wavelength of 514.5 nm and laser power of 20 mW respectively. Surface morphology and elemental composition of samples were examined by field emission scanning electron microscopy (FESEMFEI Quanta 200) and energy-dispersive X-ray spectroscopy (EDX) attached to the microscope. Optical characteristics were examined by photoluminescence at room temperature using He-Cd (325 nm) laser as excitation source. The carrier concentration of the sample was measured by using four point probes Hall measurement system.

3 Results and discussion

3.1 X-ray diffraction studies

The crystalline structure of the grown samples was analyzed using X- ray diffraction, which is shown in figure (1). InN deposited on both glass and Si substrate has the diffraction peaks that matches well with Wurtzite structure

of single phase polycrystalline InN. The lattice parameters were calculated using XRD data are a = 0.353 and c = 0.57 nm which are in good agreement with the literature values of a = 0.354 and c = 0.571 nm respectively [16].

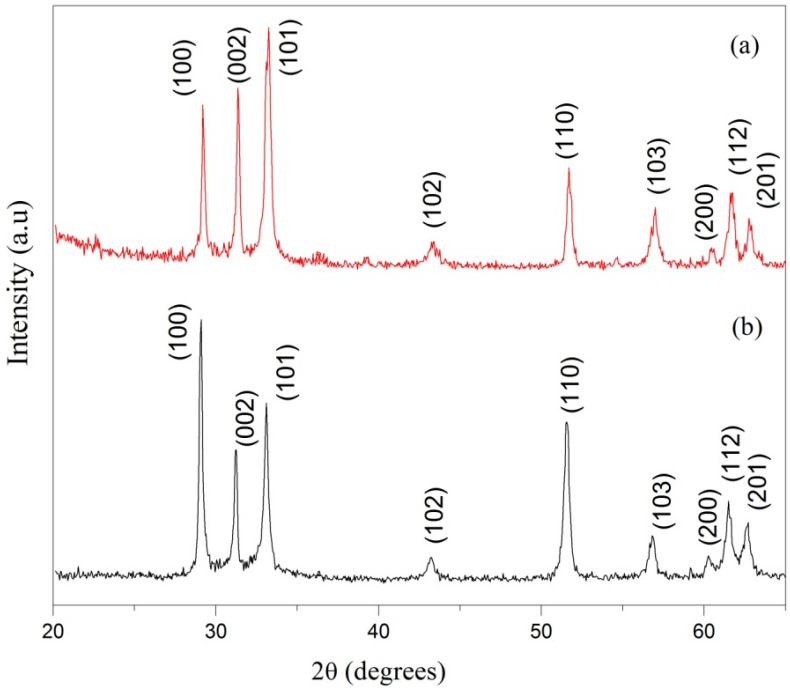

Fig 1 XRD pattern for InN thin film deposited on Si (a) and glass (b) substrates

The average crystallite size was calculated from XRD peak width of (002) based on the Debye– Scherrer equation [17].

$$D = \frac{K\lambda}{\beta \cos\theta} \qquad (1)$$

Where β is full width half maximum (FWHM) of (002) peak, K is a constant equal to 0.9, λ is the wavelength of incident x-ray (λ = 0.154 nm), D is the crystal size and θ is bragg angle. The average crystallite size calculated for InN nanocrystals deposited on glass and Si are 38 and 36 nm respectively.

3.2 Micro Raman spectroscopy

Figure (2) shows the micro Raman spectrum of InN thin films deposited on Si and glass substrates. InN has wurtzite structure and it is belongs to C^4_{6v} space group. For the measurements the lasers beam incident normal to the surface. The peaks for InN deposited on Si substrate observed at 580 and 195 cm^{-1}. The peak at 580 cm^{-1} assigned to A_1 (LO) phonon mode and its coupled with two low frequency phonon modes of A_1 (TO) at 458 cm^{-1} and E_2 (high) at 498 cm^{-1} respectively. Whereas for InN deposited on glass substrate, the peaks are observed at 574, 499 and 454 cm^{-1} which are assigned to A_1 (LO), E_2 (high) and A_1 (TO) modes respectively.

The small variation in the InN peak positions on glass substrate when compared to Si may be related to more strain relaxation in amorphous glass substrate. The broad peak observed between 150 and ended at 230 cm^{-1} with a peak maximum of 190 cm^{-1} is assigned to be B_2 (low) which is dominated by the overtones of acoustic phonon modes. All the peaks observed related to InN deposited on both the substrates were in good agreement with the literature [18, 19].

3.3 Morphological and composition Analysis

The morphology of the InN thin films deposited on both glass and Si (111) substrate were examined by field emission scanning electron microscope (FESEM) which is shown in figure 3. It is clear from the images that InN has a non-continuous morphology and the film consists of agglomerated nanocrystals. InN nanocrystals on glass have hexagonal shape facets with non-uniform size distribution as clearly seen from the higher magnification SEM images in the inset fig of 3, whereas on Si (111) substrate the morphology of the InN nanocrystals are non faceted

with rounded edges.

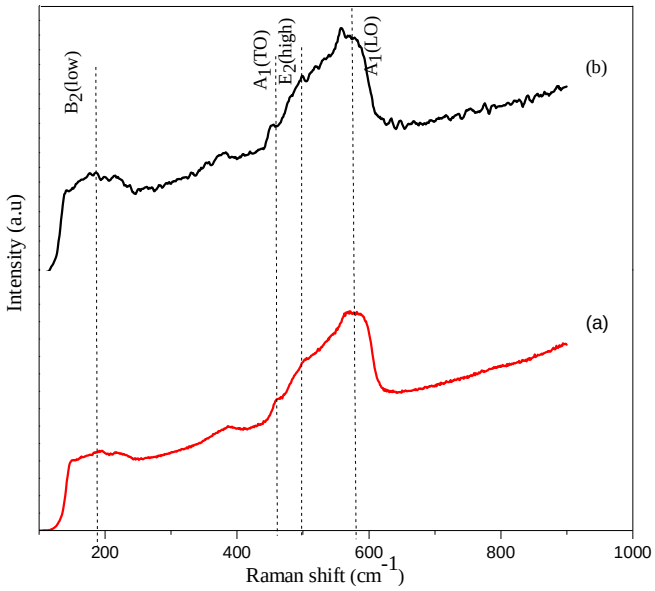

Fig 2 Micro Raman spectra of InN thin films deposited on (a) Si and (b) glass substrates

The variation in morphology due to the substrate effect, Si substrate used for the deposition is single crystalline with preferred orientation (111) whereas the glass is amorphous in nature, so the direct deposition of InN without any buffer layer on glass results in nanocrystals that are randomly distributed. However at different places on glass substrate shows some hexagonal shape micro crystals were observed with different alignment angles to the surface of the glass substrates (not shown in the article). The agglomeration was higher on Si substrate compared to the glass substrate this effect may be due to epitaxial relationship of the growth process, the adatom migrate a certain distance on the substrate surface to find favorable site, before finding the most favorable growth site these atoms or ions have the tendency to agglomerate due to the high deposition rate, short deposition time, and low mobility of adatoms on the surface of Si substrate compared to glass. The elemental composition of the InN thin films were analyzed by EDX analysis and the measurement was performed at different places of the InN thinfilm shows that the InN films are compositionally nitrogen-rich. InN thin film deposited on both the substrates contains In and N, the In to N ratios are found to be on glass and Si substrate are 1:1.2 and 1: 1.7 respectively. The impurities like oxygen and carbon also found in small fraction (less than 3%) on the InN thin films deposited on both the substrates.

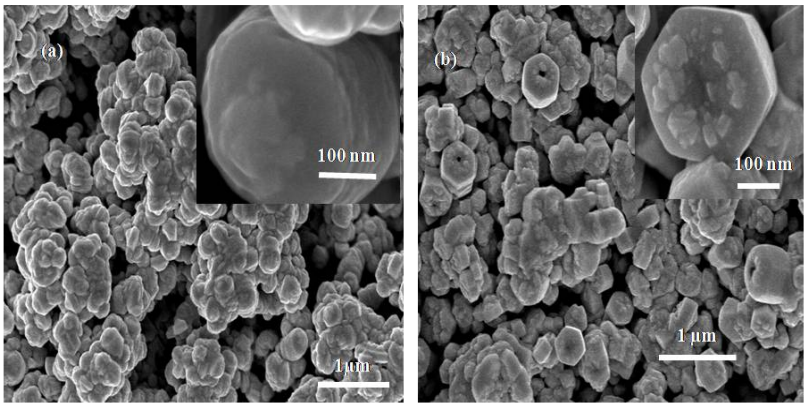

Fig 3 FESEM images of InN thin film deposited on Si (a&c) and (b) glass substrates

3.4 Photoluminescence (PL)

The PL spectrum of InN nanocrystals deposited on Si and glass substrates are shown in figure (4). The reported near band edge emission of single crystalline InN epitaxial films varies between 0.64-2.0 eV depending on the quality of the epilayers. Various mechanisms have been proposed to account the change in bandgap of InN such as the incorporation of oxygen, Moss- Burstein effect, quantum confinement effect, the strain effect and non-stoichiometry [20-23]. The deposited InN nanocrystals revealed two broad emission peaks one around 2 eV which is the near band edge of the InN nanocrystals grown under these conditions by plasma assisted reactive evaporation and another broad band around 1 eV which is realted to the deeplevel defects in the InN nanocrystals. This broad emission peaks suggest that these InN nanocrystals can be usefull for hydrogen evolution by water splitting through electrochemical and photoelectrochemical process. This spectrum of InN nanocrystals on glass is comparable with that of the InN on Si(111) substrate and corroborates with the previously reported bandgap values [15]. The bandgap of 2 eV obtained in this work as against the 0.65 eV bandgap of InN can be attributed to different effects. Such as higher carrier concentration, also referred to as the Moss Burstein shift and quantum size effect [24].

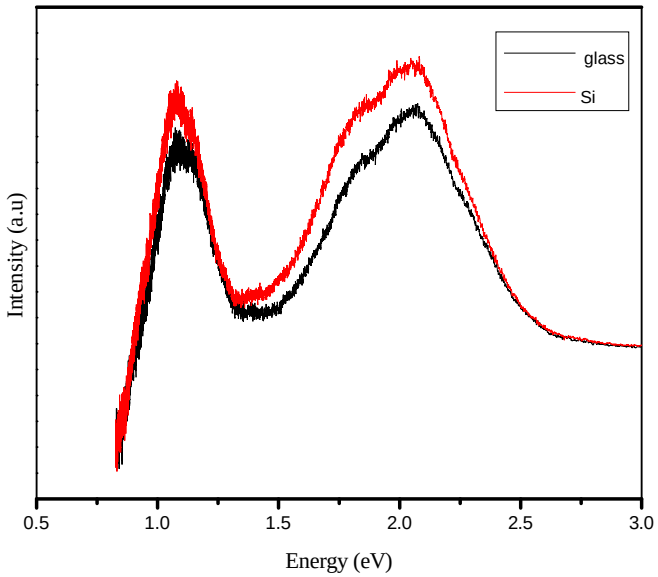

Fig 4 PL spectrum of InN thin films deposited by plasma assisted reactive evaporation on glass and Si substrates

According to Wu et al [25], due to the small effective mass of InN, the Fermi surface in the conduction band shows a strong dependence on the free electron concentration. Thus, free electrons can shift the absorption edge and PL peak to higher energy due to the band filling effect and is known as the Burstein-Moss shift. This higher bandgap value obtained is close to the previously reported value of the bandgap of InN, which was attributed by some researchers to the presense of oxygen impurity that cannot be neglected in our case also. [21, 26-29]

3.5 Hall measurement

Hall effect measurement was performed to study the electrical characteristics of plasma assisted reactive evaporation grown InN thin films deposited on both glass and Si substrates to confirm the PL results. InN thin films deposited on both the substrates shows n-type behavior. The observed carrier concentration of InN thin films on Si (sheet-1.78 $\times 10^{18}$, bulk- 1.78 $\times 10^{23}$ cm^{-3}) and glass (sheet-3.7 $\times$ 10^{17}, bulk -1.89 $\times$ 10^{21} cm^{-3}) are quite higher than the previous reporters [1, 25]. Many theoretical and experimental studies have focused on determining the major reason for the unintentional n-type conductivity of InN however no consensus has yet been reached. The general or possible reason for this high back ground concentration may be due to donor impurities or donor type native defects. The impurities most commonly suggested as the primary cause of InN's n-type conductivity are oxygen and hydrogen [25]. Among native defects, the nitrogen vacancy has been found from theoretical calculations to be a donor and has also been suggested as the major reason for the high n-type conductivity [1], but the EDX results confirms that the deposited films are nitrogen rich InN, so the origin of n-type conductivity from the sample can be due to the presence of oxygen, and other stoichiometry related defects. Impurities accumulation and native defects also play important role in producing n-type conductivity in as deposited InN thin films.

4 Conclusion

InN nanocrystals were successfully deposited on glass substrates by plasma assisted reactive evaporation system. The characteristics of In N were studied with XRD, micro Raman analysis, Pl and Hall effect measurements and compared with InN on Si (111). The hexagonal shaped InN crystals were found on glass substrates. The PL spectrum shows broad emissions at IR (2 eV) the reason for high bandgap value obtained may be due to high electron carrier concentration which leads to Burstein-Moss shift increasing the bandgap or presence of oxygen impurity. Hall measurements confirm that the samples deposited on both the substrates are n-type and has high background carrier concentration. These encouraging results suggest that the good quality InN thinfilms can be obtained on glass substrates and can be effectively used towards low cost water splitting-hydrogen evolution devices and other renewable energy resources.

Acknowledgements

The author acknowledges the DST-SERB, govt of India, for the grant (YSS/2015/000651) awarded under Young scientist scheme. This supported by the Ministry of Higher Education of Malaysia, for UM/MOHE High Impact Research Grant Allocation of F000006-21001, Exploratory Research Grant Scheme (ERGS) ER012-2011A, Fundamental Research Grant Scheme (FRGS) FP009-2013A & FP009-2013B and Universiti Malaya Research Grant (UMRG) RG141-11AFR.

References

1. A. G. Bhuiyan, A. Hashimoto, A. Yamamoto, J. Appl. Phys. **94**, 2779-2808 (2003).
2. C. S. Gallinat, G. Koblmüller, J. S. Brown, S. Bernardis, J. S. Speck, G. D. Chern Appl. Phys. Lett. **89**, 032109-3 (2006).
3. S. Suihkonen, J. Sormunen, V.T. Rangel-Kuoppa, H. Koskenvaara, M. Sopanen J. Crystal. Growth 291, 8-11 (2006).
4. J. Kamimura, K. Kishino and A. Kikuch J. App. Phys **117**, 084314-6 (2015).
5. A. L. Syrkin, V. Ivantsov, A. Usikov, V. A. Dmitriev, G. Chambard, P. Ruterana, A. V. Davydov, phys. stat. sol. (c) **5**, 1792-1794 (2008).
6. Xu Ji, Shuang Cheng, Hairong Hu, Huajun Li, and Zhiguo Wu, Appl.Phys. Lett. 2, 022150-7 (2012).
7. M. V. S. da Silva, D. G. F. David, I. Pepe, A. F. Silva, Thin Solid films. **520**, 4848-4852 (2012).
8. T. F. G. Muller, D. Knoesen, C. Arendse, R. Swanepoel, S. Halindintwali, C. Theron, Thin Solid Films. **501**, 98-101 (2006).
9. N.P. Tandian, and E. Pfender Plasma Chem. Plasma Proc. **17**, 353-370 (1997).
10. H. Kerstena, H. Deutscha, H. Steffena, G.M. W. Kroesenb and R. Hippler, Vacuum. **63**, 385-431 (2001).
11. K. Ostrikov, Rev. Mod. Phys. **77**, 489-511 (2005).
12. I. Levchenko, K. Ostrikov, K. Diwan, K. Winkler and D. Mariotti, Appl. Phys. Lett. **93**, 183102-3 (2008).
13. K. Ostrikov, I. Levchenko and S. Xu, Pure Appl. Chem. **80**, 1909-1918 (2008).
14. M. Alizadeh, H. Mehdipour, B.T. Goh and S.A. Rahman, J. Appl. Phys. **114,** 024301-8 (2013).
15. V. Ganesh, M. Alizadeh, A. Shuhaimi, A. Pandikumar, B. T. Goh, N. M. Huang, S. A. Rahman, RSC Adv. **5**, 17325-17335 (2015).
16. M. S. Hu, G. M. Hsu, K. H. Chen, C.J. Yu, APPl. Phys. Lett. **90**, 123109-3 (2007).
17. P. Bindu, Sabu Thomas J. Theor Appl Phys **8**, 123-134 (2014).
18. T. Inushima, T. Shiraishi, and V. Yu. Davydov, Solid State Commun. **110**, 491(1999) .
19. G. Kaczmarczyk, A. Kaschner, S. Reich, A. Hoffmann, C. Thomsen, D. J. As, and H. Riechert. Appl. phys. lett. **76**, 2122-2124 (2000).
20. C. K. Chao, H.-S. Chang, T. M. Hsu, C. N. Hsiao, C. C. Kei, S. Y. Kuo, and J.-I. Chyi, Nanotechnology. **17**, 3930-3932 (2006).
21. M. Yoshimoto, H. Yamamoto, W. Huang, H. Harima, J. Saraie, A.Chayahara, and Y. Horino, Appl. Phys. Lett. **83**, 3480-3482 (2003).
22. A. G. Bhuiyan, K. Sugita, K. Kasashima, A. Hashimoto, A. Yamamoto, and V. Yu. Davydov Appl. Phys. Lett. **83**, 4788-4790 (2003).
23. V. M. Naik, R. Naik, D. B. Haddad, J. S. Thakur, G. W. Auner, H. Lu, and W. J. Schaff, Appl. Phys. Lett. **86**, 201913-3 (2005).
24. W. C. Ke, C. P. Fu, C. Y. Chen, L. Lee, C. S. Ku, W. C. Chou, W.-H. Chang, M. C. Lee, W. K. Chen, W. J. Lin, Appl. phys. lett. **88**, 191913-3 (2006).

25. J. Wu, W. Walukiewicz, S. X. Li, R. Armitage, and J. C. Ho, Appl. Phys. Lett. **84**, 2805-2807 (2004).
26. T. V. Shubina, S. V. Ivanov, V. N. Jmerik, D. D. Solnyshkov, V. A. Vekshin, and B. Monemar, Phys. Rev. Lett. **92**, 117407-4 (2004).
27. S. Valdueza-Felip, F.B. Naranjo, M. Gonzalez-Herraez, L. Lahourcade, E. Monroy, S. Fernandez. J. Cryst. Growth **312**, 2689-2694 (2010).
28. M. Amirhoseiny, Z. Hassan, and S. S. Ng Vacuum. **101**, 217-220 (2014).
29. Hyun Jong Park, Olga Kryliouk, Tim Anderson, Physica E **37**, 142-147 (2007).